Fluctuations of entropy production of a run-and-tumble particle

Prajwal Padmanabha,[1] Daniel Maria Busiello,[2, *] Amos Maritan,[1] and Deepak Gupta[3, 4]

[1] *Department of Physics and Astronomy "G. Galilei", University of Padova, Padova 35131, Italy*
[2] *Ecole Polytechnique Fédérale de Lausanne (EPFL), 1015 Lausanne, Switzerland*
[3] *Department of Physics, Simon Fraser University, Burnaby, British Columbia V5A 1S6, Canada*
[4] *Institute for Theoretical Physics, Technical University of Berlin, Hardenbergstr. 36, D-10623 Berlin, Germany*

Out-of-equilibrium systems continuously generate entropy, with its rate of production being a fingerprint of non-equilibrium conditions. In small-scale dissipative systems subject to thermal noise, fluctuations of entropy production are significant. Hitherto, mean and variance have been abundantly studied, even if higher moments might be important to fully characterize the system of interest. Here, we introduce a graphical method to compute any moment of entropy production for a generic discrete-state system. Then, we focus on a paradigmatic model of active particles, i.e., run-and-tumble dynamics, which resembles the motion observed in several microorganisms. Employing our framework, we compute the first three cumulants of the entropy production for a discrete version of this model. We also compare our analytical results with numerical simulations. We find that as the number of states increases, the distribution of entropy production deviates from a Gaussian. Finally, we extend our framework to a continuous state-space run-and-tumble model, using an appropriate scaling of the transition rates. The approach here presented might help uncover the features of non-equilibrium fluctuations of any current in biological systems operating out-of-equilibrium.

I. INTRODUCTION

Biological systems are often found out of equilibrium, constantly consuming energy to maintain a stationary state [1, 2]. A large number of studies have been performed on non-equilibrium properties that such systems display [3–5]. One of the most relevant signatures of a non-equilibrium condition is the net production of entropy. At equilibrium, due to the time-reversal symmetry, a forward trajectory is equally probable compared to its time-reversed counterpart. Non-equilibrium conditions break this symmetry, leading to entropy production. This has been closely investigated, especially in the context of biological systems, to quantify their distance from thermodynamic equilibrium [6, 7]. Even outside the context of biological systems, entropy production and its features have been extensively studied [8–12].

Moreover, investigating macroscopic emergent behaviors is usually not enough in the realms of biological and biochemical systems. In fact, thermal fluctuations are prominent in small-scale systems. Therefore, researchers have investigated fluctuations of different thermodynamic quantities, such as work done [13–15], entropy production [16–19], heat flow [15, 20–22], and stochastic efficiency [23–27] within the framework of stochastic thermodynamics [8, 28, 29].

In stark contrast to equilibrium systems, basic principles are constantly being searched for in non-equilibrium systems. Stochastic thermodynamics provides a window into the possibilities of out-of-equilibrium universal laws through several seminal results, such as the fluctuation theorems [30–33], the Jarzynski equality [34], the Crooks work-fluctuation theorem [31, 35], the non-equilibrium linear response [36, 37], and the thermodynamic uncertainty relations [38–41].

In particular, entropy production and its fluctuations play a prominent role in linear response theory, fluctuation theorems, and thermodynamic uncertainty relations. In this context, various studies have focused on the estimation of the mean entropy production, both theoretically and experimentally, by using different methods, such as uncertainty relations [42–44], waiting-time distributions [45], machine learning [46], and stochastic single-trajectory data [47–49]. While an explosion of research investigate the mean entropy production, there is a lack of general understanding of the properties of its probability density function (pdf). Nevertheless, researchers have obtained the distribution of entropy production for specific settings using analytical [50–52], numerical [53], and experimental techniques [54–57].

Having an estimate for the moments of the entropy production might be as important as quantifying its mean. Though a system might be close to equilibrium, it can potentially have large fluctuations of entropy production. In fact, estimating the entire pdf provides information about this variability [58]. From a general perspective, our understanding of biological and chemical systems might benefit from the knowledge of fluctuations of any thermodynamic quantity, including entropy production [7, 59–63]. Following this research direction, in [64] the authors introduce a method to infer mean and variance of entropy production from short-time experiments, while in [55] these quantities are estimated numerically using differential equations for moments of dissipated heat, following [65]. Some studies place bounds on all steady-state currents, including entropy production [66], specifically through techniques of linear response theory [67], and large deviation theory [40]. To the best of our knowledge,

* current address: Max Planck Institute for the Physics of Complex Systems, 01187 Dresden, Germany

there exists no theoretical framework to compute the distribution of entropy production which applies to a large class of systems. One of the difficulties encountered is that entropy production is a trajectory-dependent quantity, a property that makes the analytical computation of its statistics beyond the mean a difficult task.

In the study of non-equilibrium systems, modeling of active self-propelled particles has recently been one of the most active fields. These particles break detailed balance via a self-driven term that leads to a wide range of non-equilibrium phenomena resembling various distinctive properties of living systems [68–70]. Examples of such phenomena include self assembly [71, 72], spontaneous segregation [73], and motility induced phase separation [74, 75]. The non-equilibrium nature of such systems automatically leads to questions about the properties of their thermodynamic features. Fluctuation theorems in active Ornstein-Uhlenbeck processes [76–78], stochastic thermodynamics of active particles [79, 80], their entropy production [81–85], heat fluctuations of interacting active particles [86], and experimental measurements of uncertainty relations [87] are only a few examples of works performed in this area.

One of the most studied models for active matter components is the run-and-tumble motion. Particles undergoing this dynamics capture the typical homonymous behavior displayed by microorganisms, such as *E. Coli* and *Salmonella*, characterized by driven diffusive dynamics (run) interspersed by random changes of the velocity direction (tumble) [88, 89]. In its simplest form, the model consists of a random walker whose velocity direction is influenced by a dichotomous noise [90, 91], often referred to as 'telegraphic' noise [92], and the walker's position is described by the telegrapher's equation (also relevant in electronics [93, 94]). In addition to displaying motion similar to microorganisms, run-and-tumble particles exhibit interesting steady states [91, 95] which also leads to clustering near the boundaries [89]. Recent studies have also investigated the first passage properties of this system with [94] and without stochastic resetting [96].

Run-and-tumble particles have been shown to have non-zero average entropy production [97]. Due to their popularity, the dynamics might serve as a paradigmatic model to study active matter systems. Here, we start from a discrete-state version of a model for run-and-tumble particles (Sec. II) and present a graphical method to compute cumulants of the entropy production at any order (Sec. III). Notice that, although the graphical method is employed to study the run-and-tumble setup, it is nevertheless valid for any Markovian system. We proceed to calculate analytically the third cumulant of the entropy production in this model, and verify it through simulations of the system (Sec. IV). Although obtaining the full distribution remains a lofty goal, our formalism can be, in principle, extended up to a desired precision.

Furthermore, for the given model, we find an interesting system-size scaling of the entropy production's com-

plementary cumulative distribution function. We emphasize that the approach presented here can be easily generalized to any discrete-state system (both undergoing discrete- and continuous-time evolution) and different boundary conditions. Finally in Sec. V, by implementing a proper coarse-graining procedure, we show that our predictions are compatible with those numerically obtained from the Langevin equation of run-and-tumble particles.

II. SETUP

We consider a run-and-tumble walker on a discrete state-space with reflecting boundary states. The walker hops with a switching rate r between two lanes, representing two different velocity directions in a one-dimensional system. On the upper (lower) lane, the walker hops forward with a rate a (b), and backward with a rate b (a). Without loss of generality, we consider $a > b$. The schematic diagram describing the system is shown in Fig. 1. Thus, the system consists of $2N$ states, of which N states are in the $+$ regime (i.e., upper lane), and the remaining N are in the $-$ regime (i.e., lower lane). Here '+' and '-' correspond to the direction in which the walker hops on average.
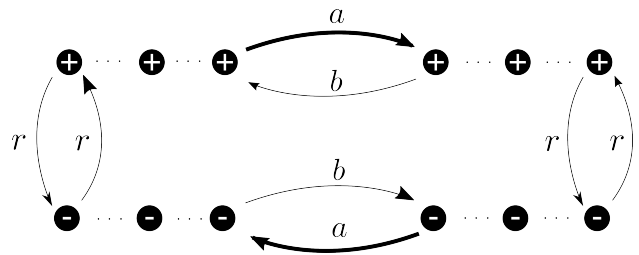

FIG. 1. Schematic representation of a run-and-tumble particle. Top layer: $+$ regime. Bottom layer: - regime. The particle hops forward and backward, respectively, with a rate a (b) and b (a) in the $+$ (-) regime, where $a > b$. Moreover, the particle switches states in between the two layers with a rate r.

The master equation governing the probability of finding a particle in the i-th state is [98]

$$\dot{P}(i,t) = \sum_j W_{ij} \, P(j,t), \qquad (1)$$

where the dot indicates the time-derivative. $W_{ij} \equiv W_{i\leftarrow j}$ is transition rate from the state j to i, $j \neq i$, and the element of the transition rate matrix $\hat{W}$ in the position (ij). Since the probability distribution is normalized at all times, i.e., $\sum_i P(i,t) = 1$, the sum of elements of each column of $\hat{W}$ is zero: $\sum_i W_{ij} = 0$ which gives $W_{jj} = -\sum_{i\neq j} W_{ij}$. Herein, we consider a system in which if $W_{ij} \neq 0$, so is W_{ji}, since there are no unidirectional transitions.

In this paper, we aim to compute fluctuations of entropy production of a run-and-tumble particle. In the case of a discrete state-space, the total entropy production, Σ_{tot}, at the level of a single trajectory is defined as follows. Given a forward trajectory $\Gamma \equiv \{(i_0, t_0), (i_1, t_1), \ldots, (i_M, t_M)\}$, where the state i_k is visited at time t_k and changes to state i_{k+1} at time t_{k+1}, the asymmetry between the probability of forward and reverse trajectories quantifies the total entropy production [8, 28, 99, 100]:

$$\Sigma_{\text{tot}}(\Gamma) \equiv \ln \frac{\mathscr{P}(\Gamma)}{\mathscr{P}(\Gamma^\dagger)}, \qquad (2)$$

where $\mathscr{P}(\Gamma)$ and $\mathscr{P}(\Gamma^\dagger)$, respectively, are the probabilities of observing a forward and a time-reversed trajectory. Note that this definition of entropy production is valid when the local detailed balance is satisfied, which we shall assume to be the case [101, 102]. In the event of local detailed balance violated, informatic entropy production needs to be considered [103]. Following [104], the total entropy production along the trajectory Γ reads:

$$\Sigma_{\text{tot}}(\Gamma) = \ln \left[\frac{P(i_0, t_0)}{P(i_M, t_M)} \prod_{i,j \in \Gamma} \left(\frac{W_{ij}}{W_{ji}} \right)^{n_{ij}} \right], \qquad (3)$$

where $P(i_0, t_0)$ and $P(i_M, t_M)$, respectively, are the probabilities of initial and final states of the trajectory, and $n_{ij} \equiv n_{i \leftarrow j}$ counts the number of jumps from the state j to i in the trajectory Γ. Σ_{tot} can be split into two contributions: system entropy production Σ_{sys}, and environment entropy production Σ_{env}. In particular, Σ_{env} is associated with the heat dissipated by the particle into the surrounding bath along the trajectory Γ:

$$\Sigma_{\text{env}}(\Gamma) \equiv \sum_{i,j \in \Gamma} n_{ij} \ln \frac{W_{ij}}{W_{ji}}, \qquad (4)$$

where j precedes i in the trajectory Γ. This is the only term that survives in the stationary state, when averaged over many trajectories [104]. Additionally, for any finite discrete-state systems, $\Sigma_{\text{sys}} = \Sigma_{\text{tot}} - \Sigma_{\text{env}}$ is a boundary term involving the initial and final states for each trajectory, and is the sub-leading contribution to the total entropy production in the long-time limit.

Since the number of jumps, n_{ij}, performed by the run-and-tumble walker is a trajectory-dependent quantity, i.e., it varies from one realization to another, the knowledge of its statistics is required to obtain the fluctuations of the entropy production in Eq. (4).

III. COMPUTATION OF CUMULANTS OF ENTROPY PRODUCTION

To compute the various correlations of the number of jumps, we start from a simpler dynamical model: a Markov chain [105, 106]. Unlike the master equation in which time changes continuously, now the time increases in discrete steps, Δt. In one time increment, the transition probability of the system to jump from the state j to i is $\mathcal{P}(i, t + \Delta t | j, t) \equiv A_{ij} = W_{ij} \Delta t$ for $i \neq j$, and the probability of staying in the state i is $A_{ii} = 1 - \sum_{j \neq i} W_{ji} \Delta t = 1 + W_{ii} \Delta t$. It follows that the sum of the elements of each column is unity, i.e., $\sum_i A_{ij} = 1$. Therefore, the Markov chain equation is

$$P(i, t + \Delta t) = \sum_{j=1}^{2N} A_{ij} P(j, t). \qquad (5)$$

In the limit $\Delta t \to 0$, the above equation (5) reduces to the master equation (1). Note that herein we are considering time-independent transition rates.

Since the time evolution runs only over times multiple of Δt, fixing the observation time T is equivalent to fixing the total number of jumps to $T/\Delta t$. In a Markov chain, time is a bookkeeping measure, and therefore, we are able to consider equally spaced time intervals for the trajectory. Hence, the probability of a Markov chain (MC) trajectory $\Gamma_{\text{MC}} \equiv \{(i_0, t_0), (i_1, t_1), \ldots, (i_M, t_M)\}$, where $t_{k+1} = t_0 + (k+1)\Delta t$ is:

$$\mathscr{P}(\Gamma_{\text{MC}}) \equiv A_{i_M i_{M-1}} A_{i_{M-1} i_{M-2}} \cdots A_{i_2 i_1} A_{i_1 i_0} P(i_0, 0), \qquad (6)$$

where $P(i_0, 0)$ is the initial probability distribution of the run-and-tumble walker at time $t_0 = 0$. Note that in Eq. (6), it is possible that $i_{k+1} = i_k$ for some k's, i.e., there is a possibility of staying in the same state after the time interval Δt which is a consequence of imposing M equally spaced time intervals. When we move back to the master equation, these probabilities of staying in the same state lead to exponential waiting time distributions of times between jumps from one state to another, thereby Γ_{MC} converges to Γ.

The path probability, $\mathscr{P}(\Gamma_{\text{MC}})$, is normalized over all trajectories, i.e.,

$$\sum_{\Gamma_{\text{MC}}} \mathscr{P}(\Gamma_{\text{MC}}) = \sum_{i_M, i_{M-1}, \ldots, i_1, i_0} A_{i_M i_{M-1}} A_{i_{M-1} i_{M-2}} \cdots$$
$$\times A_{i_2 i_1} A_{i_1 i_0} P(i_0, 0) = 1,$$

where we used $\sum_i A_{ij} = 1$ for each summation.

The number of jumps performed up to the time T across a link from ℓ to m in a trajectory Γ is then:

$$n_{m\ell}(\Gamma_{\text{MC}}) \equiv \sum_{k=0}^{M-1} \delta_{i_{k+1}, m} \ \delta_{i_k, \ell}, \qquad (7)$$

where the Kronecker deltas give 1 whenever the system performs jumps from state ℓ to m.

Let us first compute the average number of jumps over all possible trajectories:

$$\langle n_{m\ell} \rangle_{\Gamma_{\text{MC}}} = \sum_{\Gamma_{\text{MC}}} \mathscr{P}(\Gamma_{\text{MC}}) \sum_{k=0}^{M-1} \delta_{i_{k+1},m}\, \delta_{i_k,\ell} \tag{8a}$$

$$= \sum_{k=0}^{M-1} \sum_{i_M,i_{M-1},\ldots,i_1,i_0} A_{i_M i_{M-1}} A_{i_{M-1} i_{M-2}} \ldots A_{i_2 i_1} A_{i_1 i_0} P(i_0,0)\, \delta_{i_{k+1},m}\, \delta_{i_k,\ell} \tag{8b}$$

$$= \sum_{k=0}^{M-1} \sum_{i_M,\ldots,i_{k+1},i_k,i_{k-1}} A_{i_M i_{M-1}} \ldots A_{i_{k+1} i_k}\, \delta_{i_{k+1},m}\, \delta_{i_k,\ell}\, A_{i_k i_{k-1}} \sum_{i_{k-2},\ldots,i_0} A_{i_{k-1} i_{k-2}} \ldots A_{i_1 i_0} P(i_0,0) \tag{8c}$$

$$= \sum_{k=0}^{M-1} \sum_{i_{k-1},\ldots,i_0} A_{m\ell} A_{\ell i_{k-1}} A_{i_{k-1} i_{k-2}} \ldots A_{i_1 i_0} P(i_0,0) \tag{8d}$$

$$= \sum_{k=0}^{M-1} A_{m\ell}\, P(\ell,k\Delta t). \tag{8e}$$

To go from Eq. (8b) to (8c), we move the Kronecker deltas next to the $\hat{A}$'s matrix elements with the corresponding indices, and identify two groups of indices. Then, the summation over $i_M,\ldots,i_{k+2}$ gives 1 using the property $\sum_i A_{ij} = 1$, while the one over the indices $k+1$ and k can be carried out using the Kronecker delta. The resulting expression is in Eq. (8d). Finally, we use the Markov chain evolution in Eq. (5) to perform the summation on indices i_{k-1} to i_0 to obtain the last equality, Eq. (8e).

Similarly, we compute the correlations between two sets of jumps:

$$\langle n_{m\ell}\, n_{m'\ell'} \rangle_{\Gamma_{\text{MC}}} = \sum_{\Gamma_{\text{MC}}} \mathscr{P}(\Gamma_{\text{MC}}) \sum_{k=0}^{M-1} \delta_{i_{k+1},m}\, \delta_{i_k,\ell}$$
$$\times \sum_{k'=0}^{M-1} \delta_{i_{k'+1},m'}\, \delta_{i_{k'},\ell'}$$
$$= \sum_{k=0}^{M-1} \sum_{k'=0}^{M-1} \sum_{i_M,\ldots,i_0} \delta_{i_{k+1},m}\, \delta_{i_k,\ell}\, \delta_{i_{k'+1},m'}$$
$$\times\, \delta_{i_{k'},\ell'}\, A_{i_M i_{M-1}} \ldots A_{i_1 i_0} P(i_0,0).$$

We split the second summation over k' depending on three different scenarios: 1) $k' < k$, 2) $k' = k$, and 3) $k' > k$. Performing similar calculations as in the case of the first moment, we obtain, for $k' < k$,

$$\langle n_{m\ell}\, n_{m'\ell'} \rangle_{\Gamma_{\text{MC}}} = \sum_{k=0}^{M-1} \sum_{k'=0}^{k-1} A_{m\ell}\, \mathcal{P}(\ell,k\Delta t|m',(k'+1)\Delta t)$$
$$\times A_{m'\ell'}\, P(\ell',k'\Delta t), \tag{10}$$

for $k < k'$,

$$\langle n_{m\ell}\, n_{m'\ell'} \rangle_{\Gamma_{\text{MC}}} = \sum_{k=0}^{M-1} \sum_{k'=k+1}^{M-1} A_{m'\ell'}\, \mathcal{P}(\ell',k'\Delta t|m,(k+1)\Delta t)$$
$$\times A_{m\ell}\, P(\ell,k\Delta t), \tag{11}$$

and for $k' = k$,

$$\langle n_{m\ell}\, n_{m'\ell'} \rangle_{\Gamma_{\text{MC}}} = \sum_{k=0}^{M-1} A_{m\ell}\, P(\ell,k\Delta t)\, \delta_{m,m'}\delta_{\ell,\ell'}. \tag{12}$$

Combining the above three contributions, Eqs. (10), (11), and (12), finally we obtain:

$$\langle n_{m\ell}\, n_{m'\ell'} \rangle_{\Gamma_{\text{MC}}} =$$
$$\sum_{k=0}^{M-1} \Bigg[\sum_{k'=0}^{k-1} A_{m\ell}\, \mathcal{P}(\ell,k\Delta t|m',(k'+1)\Delta t) A_{m'\ell'}\, P(\ell',k'\Delta t)$$
$$+ \sum_{k'=k+1}^{M-1} A_{m'\ell'}\, \mathcal{P}(\ell',k'\Delta t|m,(k+1)\Delta t) A_{m\ell}\, P(\ell,k\Delta t)$$
$$+ A_{m\ell}\, P(\ell,k\Delta t)\delta_{m,m'}\delta_{\ell,\ell'} \Bigg]. \tag{13}$$

Such calculations become tedious on proceeding to higher order correlations. However, we present a graphical method to scale up the calculations to any order of correlations of the number of jumps. For a given correlation, we first determine the set of all possible time-orderings of k-s, i.e. the times at which a specific jump takes place. For the first moment, there is only one jump considered, hence no ordering is required. For the correlations between two sets of jumps, say $\{m,\ell\}$ and $\{m',\ell'\}$, happening at times $k\Delta t$ and $k'\Delta t$ respectively, as mentioned earlier, the possible permutations are $k < k'$, $k > k'$, and $k = k'$. Once all the orderings are listed, the set of states are graphically located according to the orderings. For example, corresponding to $k < k'$, the set of states $\{m,\ell\}$ appears before in time than the set of states $\{m',\ell'\}$. Notice that in what follows, we consider the time-axis from right to left to be consistent with the ordering at which propagators appear.

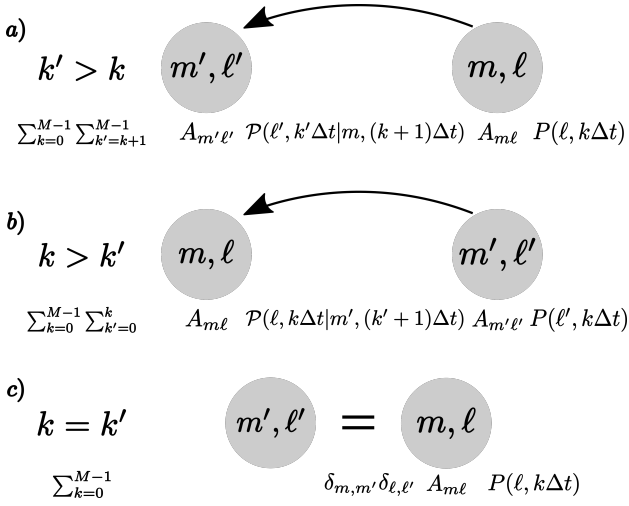Fig. 2 shows possible orderings for the second order correlation.

FIG. 2. Graphical representation for the computation of second order correlation for number of jumps. a) $k' > k$, b) $k > k'$, and c) $k' = k$. Circle indicates the set of states corresponding to the summation label, either k or k'. The arrow and equality, respectively, correspond to the transition probability from left set of states to the right ones, and the Kronecker deltas equating the set of states.

For $k' > k$ (see Fig. 2a), the rightmost circle carries a contribution from its starting state, $\{m, l\}$, at time $k\Delta t$. The contribution is equal to its probability $A_{m\ell} P(\ell, k\Delta t)$. Then the system moves towards the left circle, which is associated to the final set of states in this scenario. This transition comes with its propagator: $A_{m'\ell'} \mathcal{P}(\ell', k'\Delta t | m, (k+1)\Delta t)$. Finally the summation runs over all possible indices k and k' with the prescribed ordering ($k' > k$ in this case). Hence, we can immediately write the contribution to the second order correlation as given by Eq. (11). Similarly, we can write the contributions for $k' = k$, and $k' < k$.

For the third order correlation, repeating the graphical procedure leads to 13 possible orderings with three k-s indices (i.e., k, k', k''). We show all the orderings in Fig. 3. Writing down the summation terms according to the graphical rules, we find them to be equal to those obtained from the full calculationIn order to avoid clutter, we relegate the detailed form of the third order jump correlation to Appendix A.

To move back from a Markov chain to a master equation description, we rewrite the transition probability as $A_{m\ell} = W_{m\ell}\Delta t$, $m \neq l$, and take the limite $\Delta t \to 0$. Thus, each summation over k-s appearing in the jump correlations is converted into an integral over time, t. Although the calculations shown above are valid for an arbitrary initial condition, in what follows, we focus on the case in which the system starts from an initial steady state distribution, $P(i_0, t_0) = P^{\mathrm{st}}(i_0)$ and $P(i_M, T) = P^{\mathrm{st}}(i_M)$. Thus, the jump correlations in

Eqs. (8e) and (13) in the continuous-time limit read:

$$\langle n_{m\ell} \rangle_\Gamma = \int_0^T \mathrm{d}t\ W_{m\ell}\ P^{\mathrm{st}}(\ell), \tag{14}$$

$$\langle n_{m\ell} n_{m'\ell'} \rangle_\Gamma = \int_0^T \mathrm{d}t \left(\int_0^t \mathrm{d}t'\ W_{m\ell}\ \mathcal{P}(\ell, t | m', t')\ W_{m'\ell'} \right.$$
$$\times\ P^{\mathrm{st}}(\ell') + \int_t^T \mathrm{d}t'\ W_{m'\ell'}\ \mathcal{P}(\ell', t' | m, t)$$
$$\left. \times\ W_{m\ell}\ P^{\mathrm{st}}(\ell) \right)$$
$$+ \int_0^T \mathrm{d}t\ W_{m\ell}\ P^{\mathrm{st}}(\ell)\ \delta_{\ell, \ell'}\ \delta_{m, m'}, \tag{15}$$

where $\mathcal{P}(\ell', t' | m, t)$ is the probability to be in the state ℓ' at time t', starting from the state m at time t, computed from the master equation. The same limit can be computed for the third moment, as shown in Appendix A.

The integration on the right-hand side of first jump moment, Eq. (14), yields:

$$\langle n_{m\ell} \rangle_\Gamma = T\ W_{m\ell}\ P^{\mathrm{st}}(\ell), \tag{16}$$

whereas the computation of higher order jump moments requires the knowledge of the transition probability: $\mathcal{P}(i', t' | i, t)$. To this end, we use the eigenvector expansion of the transition rate matrix $\hat{W}$ to compute such quantity. The master equation can be written in a compact matrix form:

$$|\dot{P}(t)\rangle = \hat{W}\ |P(t)\rangle, \tag{17}$$

where $|P(t)\rangle = [P(1, t), P(2, t), \dots]^\top$ is the probability vector, and $\top$ is the matrix transpose operator. The solution of the above linear differential equation (17), given an initial state vector $|P(t_0)\rangle$, is

$$|P(t)\rangle = e^{\hat{W}(t-t_0)}|P(t_0)\rangle. \tag{18}$$

Let $\langle \psi_j |$ and $|\phi_j\rangle$, respectively, be the j-th left and right eigenvectors of the transition rate matrix, $\hat{W}$, corresponding to eigenvalue λ_j. The left and right eigenvectors satisfy the normalization condition [98]:

$$\langle \psi_j | \phi_{j'} \rangle = \delta_{j, j'}. \tag{19}$$

Expanding the right-hand side of Eq. (18) in the eigenbasis of $\hat{W}$ gives:

$$|P(t)\rangle = \sum_j \langle \psi_j | P(t_0) \rangle\ e^{-\lambda_j(t-t_0)}\ |\phi_j\rangle, \tag{20}$$

where $0 = \lambda_1 < \Re(\lambda_2) \leq \Re(\lambda_3) \leq \cdots \leq \Re(\lambda_{2N})$, where $\Re(\lambda_j)$ represents the real part of λ_j. The system considered here reaches a steady-state in the long-time limit, $|P(t \to \infty)\rangle \to |P^{\mathrm{st}}\rangle$ which is the right eigenvector corresponding to $\lambda_{j=1} = 0$ eigenvalue, i.e., $|\phi_{j=1}\rangle$. Since
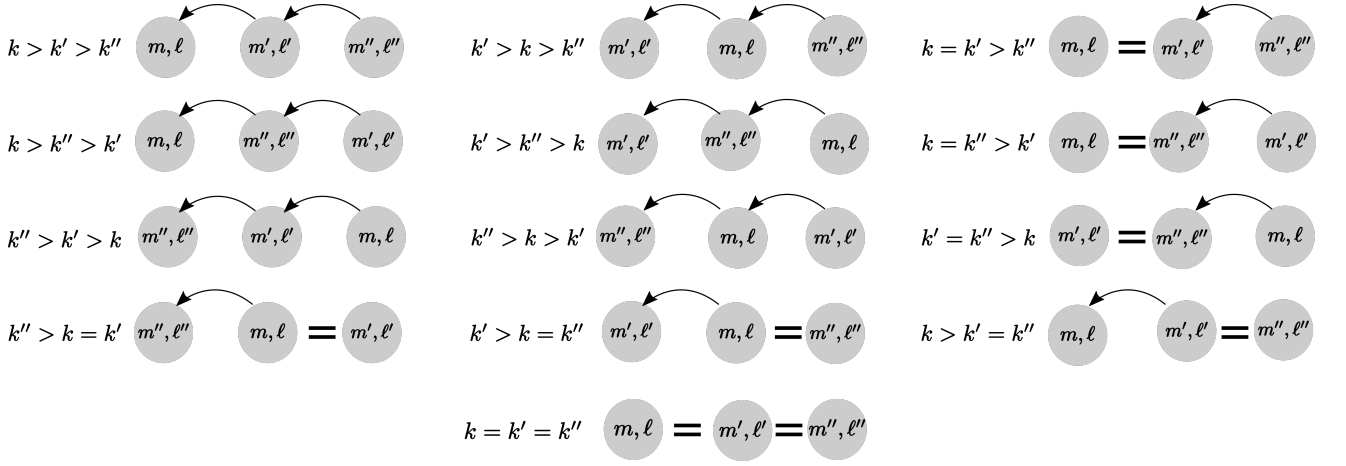
FIG. 3. Possible orderings in the graphical method for the third order correlation of number of jumps.

$\langle \psi_{j=1}|$ is a row vector with all entries equal to 1, it gives the condition $\langle \psi_{j=1}|P(t_0)\rangle = \sum_i P(i,t_0) = 1$.

In particular, if the initial state vector $|P(t_0)\rangle$ is a column vector of all zeros except 1 at i_0-th location, then the system is in the state i_0 at time t_0. Let us call this vector $|i_0\rangle$. Then, the probability of the system to be in state i at time t given the initial state i_0 at time t_0,

$\mathcal{P}(i,t|i_0,t_0) \equiv \langle i|P(t)\rangle$, can be written as:

$$\mathcal{P}(i,t|i_0,t_0) = \sum_j c_j(i_0)\, e^{-\lambda_j(t-t_0)}\, \phi_j(i), \qquad (21)$$

where we defined the projection of the left eigenvector onto the initial state as the coefficients of the expansion, i.e., $c_j(i_0) \equiv \langle \psi_j|i_0\rangle$. Similarly, we define $\phi_j(i) \equiv \langle i|\phi_j\rangle$.

Using the eigenvector expansion, Eq. (21), in the integrals appearing in Eq. (15), we obtain

$$\langle n_{m\ell}n_{m'\ell'}\rangle_\Gamma = W_{m\ell}\, W_{m'\ell'} \left[P^{\mathrm{st}}(\ell)\, P^{\mathrm{st}}(\ell')T^2 + \sum_{j>1}[c_j(m)\, \phi_j(\ell')\, P^{\mathrm{st}}(\ell) + c_j(m')\, \phi_j(\ell)\, P^{\mathrm{st}}(\ell')] \right.$$
$$\left. \times \frac{1}{\lambda_j}\left(T - \frac{1}{\lambda_j}(1 - e^{-\lambda_j T})\right) \right] + \delta_{\ell,\ell'}\, \delta_{m,m'}\, W_{m\ell}\, P^{\mathrm{st}}(\ell)\, T. \qquad (22)$$

For the third order jump correlation, let us consider an example of one of the orderings, $k < k' < k''$, with $\{m,\ell\}$, $\{m',\ell'\}$, and $\{m'',\ell''\}$ being the set of states corresponding to k, k', and k'' respectively. The contribution of this ordering is:

$$\langle n_{m,\ell}n_{m',\ell'}n_{m'',\ell''}\rangle_\Gamma = W_{m''\ell''}\, W_{m'\ell'}\, W_{m\ell}\, P^{\mathrm{st}}(\ell)$$
$$\times \sum_{j_1,j_2} \left[\phi_{j_1}(\ell'')\, c_{j_1}(m') \right.$$
$$\left. \times \phi_{j_2}(\ell')\, c_{j_2}(m)\, \mathcal{T}_{j_1,j_2} \right], \qquad (23)$$

where $\mathcal{T}_{j_1,j_2}$ represents the solution to the integral over time appearing in the third order jump correlation (see Appendix A). It is given by:

$$\mathcal{T}_{j_1,j_2} \equiv \frac{\lambda_{j_2}^2\left(1 - T\lambda_{j_1} - e^{-T\lambda_{j_1}}\right) - \lambda_{j_1}^2\left(1 - T\lambda_{j_2} - e^{-T\lambda_{j_2}}\right)}{\lambda_{j_2}^2\left(\lambda_{j_1} - \lambda_{j_2}\right)\lambda_{j_1}^2}.$$
$$(24)$$

When $\lambda_{j_1} = \lambda_{j_2}$, Eq. (24) is indeterminate. Taking L'Hôpital's rule, we find

$$\lim_{\lambda_{j_1}\to\lambda_{j_2}} \mathcal{T}_{j_1,j_2} = \frac{T\lambda_{j_1} + e^{-T\lambda_{j_1}}\left(T\lambda_{j_1} + 2\right) - 2}{\lambda_{j_1}^3}. \qquad (25)$$

Eq (24) is also indeterminate when either of the eigenvalues is zero. In such circumstances, applying L'Hôpital's rule twice, we obtain its limiting value. As an example, the limit $\lambda_{j_2} \to 0$ with $\lambda_{j_1} \neq 0$ results in the integral having the form

$$\lim_{\lambda_{j_2}\to 0} \mathcal{T}_{j_1,j_2} = \frac{2\left(1 - e^{-T\lambda_{j_1}}\right) + T\lambda_{j_1}\left(T\lambda_{j_1} - 2\right)}{2\lambda_{j_1}^3}. \qquad (26)$$

The solution (26) is similar for λ_{j_2} if $\lambda_{j_1} \to 0$ with $\lambda_{j_2} \neq 0$. If both eigenvalues are zero, i.e., $\lambda_{j_1} = \lambda_{j_2} = 0$, Eq. (24)
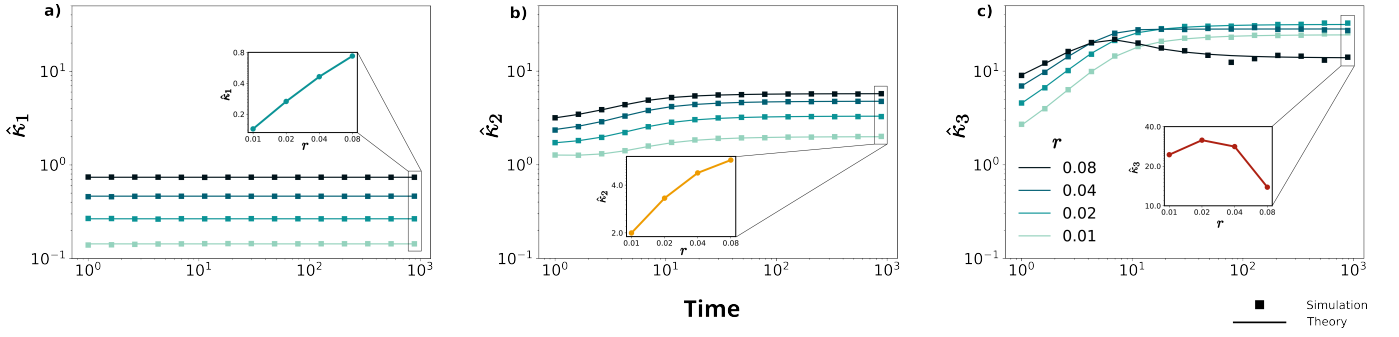
FIG. 4. Scaled cumulants of entropy production. Dots: Numerical simulation. Lines: theoretical predictions. Number of states in each regime $N = 8$, with transition rates $a = 1.0$, and $b = 0.1$. Inset shows the variation of $\hat{\kappa}_{1,2,3}$ with different switching rates r. Here the averaging is performed over 10^5 trajectories (generated using the Gillespie algorithm). In each panel, the color intensity increases with r.

results in

$$\lim_{\lambda_{j_1},\lambda_{j_2}\to 0} \mathcal{T}_{j_1,j_2} = \frac{T^3}{6}. \tag{27}$$

Notice that for all the terms in which two events happen at the same time, for example, $k_1 = k_2 < k_3$, the contribution to the n-th order jump correlation can be written in terms of the $n-1$-th order one (see Appendix A). Iterating through all possible orderings and using the solution of the time integral in Eq. (24), we can obtain the complete third order correlation for the number of jumps.

The moments and the cumulants of the environmental entropy production can be calculated from the corresponding moments and correlations for number of jumps. Indeed, for instance,

$$\kappa_1(T) \equiv \langle\Sigma_{\text{env}}(T)\rangle = \sum_{i,j}\langle n_{ij}\rangle_\Gamma \; \ln\frac{W_{ij}}{W_{ji}}, \tag{28}$$

where the i, j indices run over all $2N$ states. Scaled cumulants can then be defined as

$$\hat{\kappa}_1(T) \equiv \frac{\kappa_1(T)}{T}, \tag{29a}$$

$$\hat{\kappa}_2(T) \equiv \frac{\kappa_2(T)}{T} \equiv \frac{1}{T}\big(\langle\Sigma_{\text{env}}^2\rangle - \langle\Sigma_{\text{env}}\rangle^2\big), \tag{29b}$$

$$\hat{\kappa}_3(T) \equiv \frac{\kappa_3(T)}{T} \equiv \frac{1}{T}\big(\langle\Sigma_{\text{env}}^3\rangle - 3\langle\Sigma_{\text{env}}^2\rangle\langle\Sigma_{\text{env}}\rangle + 2\langle\Sigma_{\text{env}}\rangle^3\big), \tag{29c}$$

where the time dependence of Σ_{env} has been omitted for convenience.

We can immediately see that the first jump moment scales linearly with time as seen from Eq. (16), so does the average entropy production, $\langle\Sigma_{\text{env}}(T)\rangle$. Concerning the second cumulant, the first term on the right-hand side of Eq. (22) scales with T^2. However, this term cancels out when evaluating the cumulant, since it is equal to $\langle n_{m\ell}\rangle\langle n_{m'\ell'}\rangle$ [see Eq. (16)]. Hence, in the long-time limit, i.e., $T \gg \max(1/\lambda_j, 1 < j \le 2N)$ ($\lambda_1 = 0$ corresponding

to the stationary state), the second and third terms on the right-hand side of Eq. (22) grow linearly with the observation time T. Therefore, in this limit, the second cumulant defined in Eq. (29b) becomes

$$\langle\Sigma_{\text{env}}^2\rangle - \langle\Sigma_{\text{env}}\rangle^2 \approx T \times \sum_{i,j,k,l} f(i,j,k,l) \tag{30}$$

where $f(i, j, k, l)$ is a function that depends only on the states of the system but not on time, and can be readily determined from Eq. (22). Hence, Eqs. (29a) and (29b) give that, in the long-time limit,

$$\hat{\kappa}_1 = \text{constant}, \tag{31}$$

$$\hat{\kappa}_2 = \text{constant}. \tag{32}$$

Therefore, in any finite discrete system with bidirectional time-independent transition rates, at large times, the mean and the variance of the environmental entropy production scale linearly with time. This agrees with previous results by Lebowitz and Spohn [32] and hence, we expect all cumulants to scale linearly with time at large times, for both discrete and continuous state systems.

IV. ENTROPY PRODUCTION IN THE RUN-AND-TUMBLE MODEL

In the proposed framework, we return to the run-and-tumble model shown in Fig. 1. The transition rate matrix $\hat{W}$ has the following elements: $W_{i_+,i_++1} = b$, $W_{i_+,i_+-1} = a$, $W_{i_-,i_-+1} = a$, $W_{i_-,i_--1} = b$, $W_{i_+,i_-} = W_{i_-,i_+} = r$ with zero cross transition rates between two layers, and $W_{1_\pm,0_\pm} = 0$ and $W_{N_\pm,N_\pm+1} = 0$, where the subscript $\pm$ again denotes the respective regime of the states.

We analytically calculate the cumulants of the environmental entropy production for this system in the stationary state (up to the third cumulant, for the sake of simplicity). Furthermore, we simulate the dynamics, generating trajectories that start from the steady state, and numerically compute the entropy production. Figure 4 shows a comparison of the scaled cumulants of Σ_{env} for
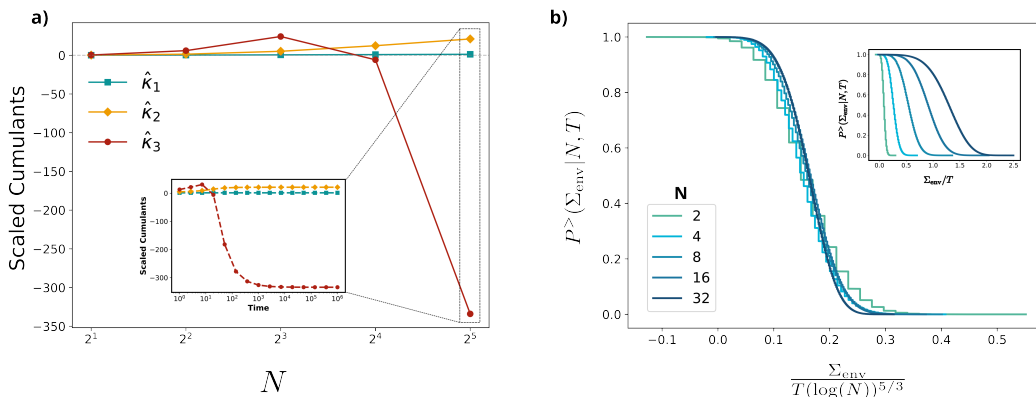
FIG. 5. a) Scaling of cumulants ($\hat{\kappa}_{1,2,3}$) of entropy production for different number of states of the discrete run-and-tumble model. Points are obtained using analytical expressions (lines serve as a visual aid to connect the dots). Inset shows the evolution of scaled cumulants against time for the system with $N = 2^5$. b) Collapse of the complementary cumulative density function (c-cdf) of entropy production, $P^>(\Sigma_{\text{env}}|N,T)$, for different number of nodes in the discrete run-and-tumble model. Entropy production at time $T = 200$ is obtained from numerical simulation using 10^6 trajectories initialized from stationary state. Inset shows the uncollapsed c-cdf, without appropriate rescaling with number of nodes. Parameters for both panels are $a = 1.0$, $b = 0.1$ and $r = 0.05$.

various values of switching rate r, obtained from analytical results with their numerical simulation counterpart. We find that each scaled cumulant reaches a stationary value in the long-time limit. The non-vanishing value of the third cumulant reflects the fact that the probability density function of the entropy production is asymmetric about its mean value.

Figure 4 also shows how $\hat{\kappa}_{1,2,3}$ change with increasing r as a function of time. We notice that the scaled average entropy production increases when the switching rate increases. This effect can be understood by realizing that, when $r \to 0$, each layer will relax to an equilibrium distribution, hence generating no entropy into the environment on average. Hence, when r increases, the system starts to feel the non-equilibrium condition that is generated by the presence of two regimes, $+$ and $-$, and the entropy production increases. Due to the same reason, the variance of the entropy production also increases with increasing r. As a second observation, the third cumulant is consistently far from zero, stressing the non-Gaussianity of the pdf of entropy production.

It is also important to analyze the scaling of the cumulants with the number of nodes, in order to investigate how the distribution of entropy production changes as a function of the system size. We analytically compute the scaled cumulants $\hat{\kappa}_{1,2,3}$ for various system sizes, starting from the steady state, and show them in Fig. 5a, while the inset shows scaled cumulants against time for the system with $N = 32$. We observe that the first two cumulants increase with N. Conversely, the sign of the third cumulant changes with N, due to the shift of mode of the distribution of entropy production with respect to its mean, i.e., skewness is positive when the mean is greater than the mode, and negative otherwise.

Then, we numerically simulate the system for dif-

ferent N, starting from the steady state, to compute the complementary cumulative density function (c-cdf), $P^>(\Sigma_{\text{env}}|N,T)$, of Σ_{env}, defined as

$$P^>(\Sigma_{\text{env}}|N,T) \equiv \int_{\Sigma_{\text{env}}}^{\infty} ds\ p_\Sigma(s|N,T). \qquad (33)$$

Here, $p_\Sigma(s|N,T)$ is the probability density function of finding the environmental entropy production to be equal to s at time T for a system of N sites in each regime. We find the leading order scaling with N of the c-cdf of Σ_{env} to be $(\ln(N))^{5/3}$. We note that this is a preliminary observation about the distribution of entropy production and warrants further studies to understand its origin.

In Fig. 5b, we show the collapse of different c-cdf for an increasing number of nodes, N. Clearly, there are also sub-leading contributions to the scaling of the moments that play a role in determining the behavior of the third cumulant shown in Fig. 5a.

Notice that increasing the number of states without scaling the rates by N does not correspond to the correct continuum limit [11]. In the next section, we present how to generalize our findings to the case of a run-and-tumble particle in a continuous domain by considering appropriate rescaling of the transition rates.

V. CONVERGENCE TO CONTINUOUS RUN-AND-TUMBLE MODEL

Let us start from the description of a particle experiencing run-and-tumble dynamics in a $1D$ continuous space $[-L, L]$, with reflecting boundary conditions. The Langevin equation describing this dynamics is [91]:

$$\dot{x} = v\ \sigma(t) + \sqrt{2D}\eta(t), \qquad (34)$$

where $\sigma(t) = \pm 1$ is a dichotomous noise that switches between $+1$ and -1 with a constant rate r, v the bare velocity of the particle in either direction in the absence of thermal noise, $D \equiv k_B \mathbb{T}/\gamma$ the diffusion constant (for k_B the Boltzmann's constant, $\mathbb{T}$ the temperature, and γ the dissipation constant), and $\eta(t)$ is the Gaussian white noise with zero mean and unit variance. The corresponding Fokker-Planck equation reads:

$$\partial_t \rho_+ = -v\,\partial_x \rho_+ + D\partial_x^2 \rho_+ - r(\rho_+ - \rho_-), \qquad (35a)$$

$$\partial_t \rho_- = +v\,\partial_x \rho_- + D\partial_x^2 \rho_- - r(\rho_- - \rho_+), \qquad (35b)$$

where ρ_+ and ρ_-, respectively, are the probability density functions for the system to be in the state $\sigma = +1$ and $\sigma = -1$, respectively, at the position x and time t [91]. For convenience, we have omitted the position and time dependence from $\rho_\pm(x,t)$.

Let us now go back to our original discrete-state description. The particle can move either in the upper or in the lower $1D$ lattices, i.e., lanes, with a rate of switching between the lanes equal to r. The master equation associated solely with the motion along the upper lane $(+)$, ignoring the switching between lanes, is:

$$\dot{P}(i_+, t) = aP(i_+ - 1, t) + bP(i_+ + 1, t) - (a+b)P(i_+, t). \qquad (36)$$

A similar equation holds also for the lower lane, interchanging a with b, following the model sketched in Fig. 1). In order to map this dynamics to a continuous space, we introduce the information that the system exists in a $1D$ box, $[-L, L]$. Hence, as we increase the number of states N in each lane, the spacing between the states has to decrease. In particular, let the spacing between the states $\delta \equiv 2L/N$. Considering again the upper lane, employing this mapping, the spatial position of the particle, $x = i_+\delta$, and the probability density function transforms as follows: $\rho_+(x) = P(i_+)/\delta = P(x/\delta)/\delta$.

A standard Kramers-Moyal expansion [105] on Eq. (36), taking δ as small parameter in the limit $N \to +\infty$, up to the second order, gives:

$$\partial_t \rho_+ = -(a-b)\delta\frac{\partial \rho_+}{\partial x} + \frac{(a+b)}{2}\delta^2\frac{\partial^2 \rho_+}{\partial x^2}. \qquad (37)$$

Performing the same expansion on the lower lane dynamics as well, and adding the switching process between these two regimes, we can compare the resulting set of coupled differential equation with Eq. (35). The matching between these two dynamical evolution becomes exact in the $N \to +\infty$ limit, when the following scaling holds:

$$a = \frac{N}{4L}\left(\frac{DN}{L} + v\right), \qquad (38a)$$

$$b = \frac{N}{4L}\left(\frac{DN}{L} - v\right). \qquad (38b)$$

It is indeed always true that when performing the continuum limit starting from a discrete-state process, the rates have to properly scaled with the number of states.

Let us now compute the thermodynamics of the continuous process. Given the Langevin equation (34), the amount of the heat absorbed by the run-and-tumble particle from the heat bath during an observation time, T, is [29]:

$$Q \equiv \int_0^T \mathrm{d}\tau \left[\sqrt{2D\gamma^2}\eta(\tau) - \gamma\dot{x}(\tau)\right] \circ \dot{x}(\tau), \qquad (39)$$

where $\circ$ denotes the Stratonovich product. In the absence of switching, the system satisfies detailed balance and reaches equilibrium. In the presence of switching, effectively, there is only an additional stochastic force on the system with respect to the equilibrium scenario. Hence, we expect the local detailed balance to hold. Thus, the environmental entropy production is [28]:

$$S_{\text{env}}(T) = \frac{\gamma}{\mathbb{T}}\int_0^T \mathrm{d}\tau \left[\dot{x}(\tau) - \sqrt{2D}\eta(\tau)\right] \circ \dot{x}(\tau). \qquad (40)$$

where we use the Einstein relation, $D = k_B \mathbb{T}/\gamma$ for $k_B = 1$. This system is known to have non zero mean entropy production rate [97].

Figure 6 shows the first two scaled cumulants of the entropy production for various system sizes, using the scaling in Eq. (38), against their value for the continuous system. In particular, the mean entropy production rate has been computed analytically in [97] while we compute the variance of S_{env} in Eq. (40) from the Langevin simulations. The convergence to the continuous case as N increases can be clearly appreciated. Furthermore, due to this convergence, we note that our assumption of local detailed balance in the discrete case is justified a-posteriori.

Unlike the mean entropy production rate, to the best of our knowledge, there have been no theoretical considerations into calculating the variance of entropy production of the run-and-tumble model in continuous space. We have shown that we can compute it using our method under appropriate scaling, and its value converges to what is observed in the continuous system. Similar procedure can also be performed for any moment of the entropy production, but the computation of the third moment in discrete-state system already scales as $\mathcal{O}(N^3)$, making its computation intensive for a large number of states.

VI. SUMMARY

In summary, first we have presented a graphical method to compute the exact moments of entropy production for any discrete-state Markovian system. Employing this method, we have shown that the first and second cumulants scale linearly with time in the long-time limit.

Then, we have applied the developed framework to predict the cumulants of the environmental entropy production in the discrete run-and-tumble model at stationarity, finding non-zero mean, variance and skewness. Additionally, increasing the system size, the environmental
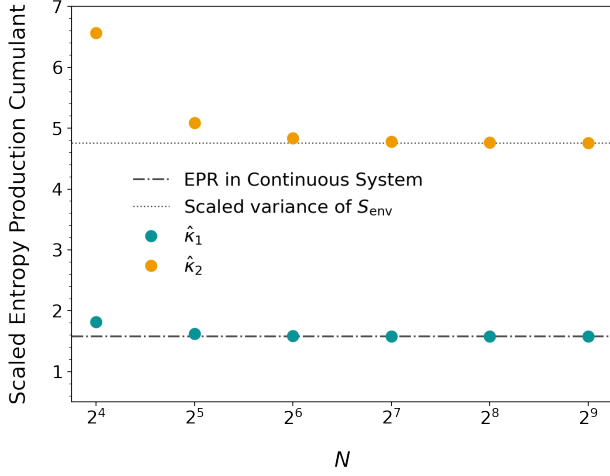
FIG. 6. Comparison between scaled cumulants of entropy production in the discrete and the continuous run-and-tumble model. The dashed line is the mean entropy production rate (EPR) given analytically in Ref. [97]. The dotted line is the variance of environmental entropy production calculated from the Langevin simulations of the continuous run-and-tumble model on 1D box within $[-5, 5]$ with velocity of the particle $v = 1.0$, diffusion coefficient $D = 0.5$, and switching rate $r = 1.0$. The points are analytically calculated scaled cumulants of environmental entropy production in the discrete run-and-tumble model with scaling of transition rates given by (38).

entropy production exhibits a remarkable non-Gaussian behavior, highlighting the potential relevance of higher moments when studying the fluctuations of discrete-state systems. Finally, we have performed the continuum limit on the proposed model, finding the correct scaling of the rates with the number of nodes. Within this description, we computed the cumulants of the environmental entropy production for a Langevin run-and-tumble model. We found striking agreement between our predictions, numerical simulations, and a theoretical result previously obtained only for the mean [97].

The graphical method presented here can be straightforwardly extended to analyze the moments of currents of any discrete-state systems (and also their continuous counterparts). Our findings suggest that cumulants other than the first two might be relevant in quantifying out-of-equilibrium fluctuations. In principle, one could try to estimate the full probability density function (pdf) of the entropy production including more than the first two moments, using a Maximum Entropy Principle. This task is usually computationally expensive even with only the first three cumulants. Hence, a smarter approach to move from cumulants to an estimation of the PDF would be an interesting topic for future investigations.

Apart from the run-and-tumble model, other common active particle models in the literature are active Brownian particles [107], and active Ornstein-Uhlenbeck particles [78]. Recently, general principles for the entropy production of these active systems have been investi-

gated [108], also in the underdamped regime [109]. While results indicated by our work and Ref. [32] give ideas about long time scaling of the cumulants, the exact details about the nature and scaling of entropy production cumulants of various active particle models is another possible line of future investigation.

Appendix A: Third order jump correlation

In order to compute the third cumulant, we require all the third order correlations for the number of jumps between states. In this section, following the graphical method, we show some of the terms that arise in this computation. From Fig. 3, we choose three orderings of different kinds, a) $k > k' > k''$ where all three k-s are different, b) $k > k' = k''$ where only two of the k-s are different, and c) $k = k' = k''$ where all three k-s are equal.

For $k > k' > k''$, the contribution to third order correlation is

$$
\begin{aligned}
\langle n_{m\ell} n_{m'\ell'} n_{m''\ell''} \rangle_{\Gamma_{\mathrm{MC}}} = &\sum_{k=0}^{M-1} \sum_{k'=0}^{k} \sum_{k''=0}^{k'} A_{m\ell} \\
&\times \mathcal{P}(\ell, k\Delta t | m', (k'+1)\Delta t) \, A_{m'\ell'} \\
&\times \mathcal{P}(\ell', k'\Delta t | m'', (k''+1)\Delta t) \\
&\times A_{m''\ell''} \, P(\ell'', k''\Delta t). \quad \text{(A1)}
\end{aligned}
$$

Similarly for $k > k' = k''$,

$$
\begin{aligned}
\langle n_{m\ell} n_{m'\ell'} n_{m''\ell''} \rangle_{\Gamma_{\mathrm{MC}}} = &\sum_{k=0}^{M-1} \sum_{k'=0}^{k} A_{m\ell} \\
&\times \mathcal{P}(\ell, k\Delta t | m', (k'+1)\Delta t) \, \delta_{m',m''} \\
&\times \delta_{\ell',\ell''} \, A_{m'\ell'} \, P(\ell', k'\Delta t), \\
&\qquad\qquad\qquad\qquad\qquad \text{(A2)}
\end{aligned}
$$

and for $k = k' = k''$,

$$
\begin{aligned}
\langle n_{m\ell} n_{m'\ell'} n_{m''\ell''} \rangle_{\Gamma_{\mathrm{MC}}} = &\sum_{k=0}^{M-1} \delta_{m,m'} \, \delta_{\ell,\ell'} \, \delta_{m',m''} \, \delta_{\ell',\ell''} \\
&\times A_{m\ell} \, P(\ell, k\Delta t) \\
= &\langle n_{m,\ell} \rangle_{\Gamma_{\mathrm{MC}}} \, \delta_{m,m'} \, \delta_{\ell,\ell'} \, \delta_{m',m''} \, \delta_{\ell',\ell''}. \\
&\qquad\qquad\qquad\qquad\qquad \text{(A3)}
\end{aligned}
$$

The contributions from $k < k' = k''$, and $k > k' = k''$ can be written in terms of the second order jump correlations and the first moment of jumps, i.e.,

$$
\begin{aligned}
\langle n_{m\ell} n_{m'\ell'} n_{m'',\ell''} \rangle_{\Gamma_{\rm MC}} = \ & \langle n_{m\ell} n_{m'\ell'} \rangle_{\Gamma_{\rm MC}} \ \delta_{m',m''} \ \delta_{\ell',\ell''} \\
& - \langle n_{m,\ell} \rangle_{\Gamma_{\rm MC}} \ \delta_{m',m''} \ \delta_{\ell',\ell''} \\
& \times \ \delta_{m',m''} \ \delta_{\ell',\ell''}
\end{aligned}
\tag{A4}
$$

Conversely, starting from a stationary state, $P^{\rm st}$, and taking the limit $\Delta t \to 0$ to recover the master equation formalism, the term arising from Eq. (A1) gives the following integral:

$$
\begin{aligned}
\langle n_{m\ell} n_{m'\ell'} n_{m'',\ell''} \rangle_T = \ & W_{ml} \ W_{m'\ell'} \ W_{m''\ell''} \ P^{\rm st}(\ell'') \\
& \times \int_0^T dt \int_0^t dt' \ \mathcal{P}(\ell, t | m', t') \\
& \times \int_0^{t'} dt'' \mathcal{P}(\ell', t' | m'', t'')
\end{aligned}
\tag{A5}
$$

Using the eigenvector expansion for the transition probability $\mathcal{P}(i, t | i_0, t_0)$ (see Eq. (21)), the integrals on the right-hand side of Eq. (A5) give $\mathcal{T}_{j_1, j_2}$, i.e, Eq. (24).

[1] Ilya Prigogine and Gregoire Nicolis. Biological order, structure and instabilities1. *Quarterly reviews of biophysics*, 4(2-3):107–148, 1971.

[2] Erwin Schrödinger. *What is Life? The Physical Aspect of the Living Cell*. Cambridge University Press, 1944.

[3] Xiaona Fang, Karsten Kruse, Ting Lu, and Jin Wang. Nonequilibrium physics in biology. *Reviews of Modern Physics*, 91(4):045004, 2019.

[4] Felix Ritort. Nonequilibrium fluctuations in small systems: From physics to biology. *Advances in chemical physics*, 137:31, 2008.

[5] Carlos Bustamante, Jan Liphardt, and Felix Ritort. The nonequilibrium thermodynamics of small systems. *arXiv preprint cond-mat/0511629*, 2005.

[6] Étienne Fodor, Cesare Nardini, Michael E Cates, Julien Tailleur, Paolo Visco, and Frédéric Van Wijland. How far from equilibrium is active matter? *Physical review letters*, 117(3):038103, 2016.

[7] Junang Li, Jordan M Horowitz, Todd R Gingrich, and Nikta Fakhri. Quantifying dissipation using fluctuating currents. *Nature communications*, 10(1):1–9, 2019.

[8] Udo Seifert. Stochastic thermodynamics, fluctuation theorems and molecular machines. *Reports on progress in physics*, 75(12):126001, 2012.

[9] Giovanni Diana and Massimiliano Esposito. Mutual entropy production in bipartite systems. *Journal of Statistical Mechanics: Theory and Experiment*, 2014(4):P04010, 2014.

[10] Daniel M Busiello, Jorge Hidalgo, and Amos Maritan. Entropy production in systems with random transition rates close to equilibrium. *Physical Review E*, 96(6):062110, 2017.

[11] Daniel M Busiello, Jorge Hidalgo, and Amos Maritan. Entropy production for coarse-grained dynamics. *New Journal of Physics*, 21(7):073004, 2019.

[12] Daniel M Busiello and Amos Maritan. Entropy production in master equations and fokker–planck equations: facing the coarse-graining and recovering the information loss. *Journal of Statistical Mechanics: Theory and Experiment*, 2019(10):104013, 2019.

[13] R Van Zon and EGD Cohen. Stationary and transient work-fluctuation theorems for a dragged brownian particle. *Physical Review E*, 67(4):046102, 2003.

[14] Frédéric Douarche, Sylvain Joubaud, Nicolas B Garnier, Artyom Petrosyan, and Sergio Ciliberto. Work fluctuation theorems for harmonic oscillators. *Physical review letters*, 97(14):140603, 2006.

[15] Sanjib Sabhapandit. Heat and work fluctuations for a harmonic oscillator. *Physical Review E*, 85(2):021108, 2012.

[16] GM Wang, Edith M Sevick, Emil Mittag, Debra J Searles, and Denis J Evans. Experimental demonstration of violations of the second law of thermodynamics for small systems and short time scales. *Physical Review Letters*, 89(5):050601, 2002.

[17] Sergio Ciliberto, Alberto Imparato, Antoine Naert, and Marius Tanase. Heat flux and entropy produced by thermal fluctuations. *Physical review letters*, 110(18):180601, 2013.

[18] Deepak Gupta and Sanjib Sabhapandit. Partial entropy production in heat transport. *Journal of Statistical Mechanics: Theory and Experiment*, 2018(6):063203, 2018.

[19] Mayank Shreshtha and Rosemary J Harris. Thermodynamic uncertainty for run-and-tumble–type processes. *EPL (Europhysics Letters)*, 126(4):40007, 2019.

[20] R. van Zon and E. G. D. Cohen. Extension of the fluctuation theorem. *Phys. Rev. Lett.*, 91:110601, Sep 2003.

[21] Paolo Visco. Work fluctuations for a brownian particle between two thermostats. *Journal of Statistical Mechanics: Theory and Experiment*, 2006(06):P06006, 2006.

[22] Anupam Kundu, Sanjib Sabhapandit, and Abhishek Dhar. Large deviations of heat flow in harmonic chains. *Journal of Statistical Mechanics: Theory and Experiment*, 2011(03):P03007, 2011.

[23] Ignacio A Martínez, Édgar Roldán, Luis Dinis, Dmitri Petrov, Juan MR Parrondo, and Raúl A Rica. Brownian carnot engine. *Nature physics*, 12(1):67–70, 2016.

[24] Christian Van den Broeck, Niraj Kumar, and Katja Lindenberg. Efficiency of isothermal molecular machines at maximum power. *Physical review letters*, 108(21):210602, 2012.

[25] Gatien Verley, Massimiliano Esposito, Tim Willaert, and Christian Van den Broeck. The unlikely carnot efficiency. *Nature communications*, 5(1):1–5, 2014.

[26] Deepak Gupta and Sanjib Sabhapandit. Stochastic efficiency of an isothermal work-to-work converter engine. *Physical Review E*, 96(4):042130, 2017.

[27] Deepak Gupta. Exact distribution for work and stochastic efficiency of an isothermal machine. *Journal of Statistical Mechanics: Theory and Experiment*, 2018(7):073201, 2018.

[28] Udo Seifert. Entropy production along a stochastic trajectory and an integral fluctuation theorem. *Physical*

review letters, 95(4):040602, 2005.

[29] Ken Sekimoto. *Stochastic energetics*, volume 799. Springer, 2010.

[30] Jorge Kurchan. Fluctuation theorem for stochastic dynamics. *Journal of Physics A: Mathematical and General*, 31(16):3719, 1998.

[31] Gavin E Crooks. Entropy production fluctuation theorem and the nonequilibrium work relation for free energy differences. *Physical Review E*, 60(3):2721, 1999.

[32] Joel L Lebowitz and Herbert Spohn. A gallavotti–cohen-type symmetry in the large deviation functional for stochastic dynamics. *Journal of Statistical Physics*, 95(1):333–365, 1999.

[33] Michele Campisi, Peter Talkner, and Peter Hänggi. Fluctuation theorem for arbitrary open quantum systems. *Physical review letters*, 102(21):210401, 2009.

[34] Christopher Jarzynski. Nonequilibrium equality for free energy differences. *Physical Review Letters*, 78(14):2690, 1997.

[35] Gavin E Crooks. Nonequilibrium measurements of free energy differences for microscopically reversible markovian systems. *Journal of Statistical Physics*, 90(5):1481–1487, 1998.

[36] Marco Baiesi and Christian Maes. An update on the nonequilibrium linear response. *New Journal of Physics*, 15(1):013004, 2013.

[37] Marco Baiesi, Christian Maes, and Bram Wynants. Fluctuations and response of nonequilibrium states. *Physical review letters*, 103(1):010602, 2009.

[38] Andreas Dechant. Multidimensional thermodynamic uncertainty relations. *Journal of Physics A: Mathematical and Theoretical*, 52(3):035001, 2018.

[39] Andre C Barato and Udo Seifert. Thermodynamic uncertainty relation for biomolecular processes. *Physical review letters*, 114(15):158101, 2015.

[40] Todd R Gingrich, Jordan M Horowitz, Nikolay Perunov, and Jeremy L England. Dissipation bounds all steady-state current fluctuations. *Physical review letters*, 116(12):120601, 2016.

[41] Jordan M Horowitz and Todd R Gingrich. Thermodynamic uncertainty relations constrain non-equilibrium fluctuations. *Nature Physics*, 16(1):15–20, 2020.

[42] Sreekanth K Manikandan, Subhrokoli Ghosh, Avijit Kundu, Biswajit Das, Vipin Agrawal, Dhrubaditya Mitra, Ayan Banerjee, and Supriya Krishnamurthy. Quantitative analysis of non-equilibrium systems from short-time experimental data. *Communications Physics*, 4(1):1–10, 2021.

[43] Biswajit Das, Sreekanth K Manikandan, and Ayan Banerjee. Inferring entropy production in anharmonic brownian gyrators. *arXiv preprint arXiv:2204.09283*, 2022.

[44] Tan Van Vu, Yoshihiko Hasegawa, et al. Entropy production estimation with optimal current. *Physical Review E*, 101(4):042138, 2020.

[45] Dominic J Skinner and Jörn Dunkel. Estimating entropy production from waiting time distributions. *Physical review letters*, 127(19):198101, 2021.

[46] Shun Otsubo, Sosuke Ito, Andreas Dechant, and Takahiro Sagawa. Estimating entropy production by machine learning of short-time fluctuating currents. *Physical Review E*, 101(6):062106, 2020.

[47] Édgar Roldán and Juan MR Parrondo. Estimating dissipation from single stationary trajectories. *Physical re-view letters*, 105(15):150607, 2010.

[48] Shun Otsubo, Sreekanth K Manikandan, Takahiro Sagawa, and Supriya Krishnamurthy. Estimating time-dependent entropy production from non-equilibrium trajectories. *Communications Physics*, 5(1):1–10, 2022.

[49] Boris Lander, Jakob Mehl, Valentin Blickle, Clemens Bechinger, and Udo Seifert. Noninvasive measurement of dissipation in colloidal systems. *Physical Review E*, 86(3):030401, 2012.

[50] Arnab Saha, Sourabh Lahiri, and AM Jayannavar. Entropy production theorems and some consequences. *Physical Review E*, 80(1):011117, 2009.

[51] Deepak Gupta and Sanjib Sabhapandit. Fluctuation theorem for entropy production of a partial system in the weak-coupling limit. *EPL (Europhysics Letters)*, 115(6):60003, 2016.

[52] Deepak Gupta and Sanjib Sabhapandit. Entropy production for partially observed harmonic systems. *Journal of Statistical Mechanics: Theory and Experiment*, 2020(1):013204, 2020.

[53] Thomas Martynec, Sabine HL Klapp, and Sarah AM Loos. Entropy production at criticality in a nonequilibrium potts model. *New Journal of Physics*, 22(9):093069, 2020.

[54] C Tietz, S Schuler, T Speck, U Seifert, and J Wrachtrup. Measurement of stochastic entropy production. *Physical review letters*, 97(5):050602, 2006.

[55] Thomas Speck, Valentin Blickle, Clemens Bechinger, and Udo Seifert. Distribution of entropy production for a colloidal particle in a nonequilibrium steady state. *EPL (Europhysics Letters)*, 79(3):30002, 2007.

[56] JV Koski, T Sagawa, OP Saira, Y Yoon, A Kutvonen, P Solinas, M Möttönen, T Ala-Nissila, and JP Pekola. Distribution of entropy production in a single-electron box. *Nature Physics*, 9(10):644–648, 2013.

[57] Sreekanth K. Manikandan, Biswajit Das, Avijit Kundu, Raunak Dey, Ayan Banerjee, and Supriya Krishnamurthy. Nonmonotonic skewness of currents in nonequilibrium steady states. *Phys. Rev. Research*, 4:043067, Oct 2022.

[58] Sergio Ciliberto. Experiments in stochastic thermodynamics: Short history and perspectives. *Physical Review X*, 7(2):021051, 2017.

[59] Daniel S Seara, Vikrant Yadav, Ian Linsmeier, A Pasha Tabatabai, Patrick W Oakes, SM Tabei, Shiladitya Banerjee, and Michael P Murrell. Entropy production rate is maximized in non-contractile actomyosin. *Nature communications*, 9(1):1–10, 2018.

[60] Sriram Ramaswamy. The mechanics and statistics of active matter. *Annu. Rev. Condens. Matter Phys.*, 1(1):323–345, 2010.

[61] Ignacio A Martinez, Édgar Roldán, Luis Dinis, and Raúl A Rica. Colloidal heat engines: a review. *Soft matter*, 13(1):22–36, 2017.

[62] Daniel M Busiello, Shiling Liang, Francesco Piazza, and Paolo De Los Rios. Dissipation-driven selection of states in non-equilibrium chemical networks. *Communications Chemistry*, 4(1):1–7, 2021.

[63] Avinash Vicholous Dass, Thomas Georgelin, Frances Westall, Frédéric Foucher, Paolo De Los Rios, Daniel M Busiello, Shiling Liang, and Francesco Piazza. Equilibrium and non-equilibrium furanose selection in the ribose isomerisation network. *Nature Communications*, 12(1):1–10, 2021.

[64] Sreekanth K Manikandan, Deepak Gupta, and Supriya Krishnamurthy. Inferring entropy production from short experiments. *Physical review letters*, 124(12):120603, 2020.

[65] Thomas Speck and Udo Seifert. Integral fluctuation theorem for the housekeeping heat. *Journal of Physics A: Mathematical and General*, 38(34):L581, 2005.

[66] Andreas Dechant and Shin-ichi Sasa. Entropic bounds on currents in langevin systems. *Physical Review E*, 97(6):062101, 2018.

[67] Patrick Pietzonka, Andre C Barato, and Udo Seifert. Universal bounds on current fluctuations. *Physical Review E*, 93(5):052145, 2016.

[68] M Cristina Marchetti, Jean-François Joanny, Sriram Ramaswamy, Tanniemola B Liverpool, Jacques Prost, Madan Rao, and R Aditi Simha. Hydrodynamics of soft active matter. *Reviews of modern physics*, 85(3):1143, 2013.

[69] Sriram Ramaswamy. Active matter. *Journal of Statistical Mechanics: Theory and Experiment*, 2017(5):054002, 2017.

[70] Jacques Prost, Frank Jülicher, and Jean-François Joanny. Active gel physics. *Nature physics*, 11(2):111–117, 2015.

[71] Joakim Stenhammar, Raphael Wittkowski, Davide Marenduzzo, and Michael E Cates. Light-induced self-assembly of active rectification devices. *Science advances*, 2(4):e1501850, 2016.

[72] Yunfei Du, Huijun Jiang, and Zhonghuai Hou. Self-assembly of active core corona particles into highly ordered and self-healing structures. *The Journal of Chemical Physics*, 151(15):154904, 2019.

[73] Joakim Stenhammar, Raphael Wittkowski, Davide Marenduzzo, and Michael E Cates. Activity-induced phase separation and self-assembly in mixtures of active and passive particles. *Physical review letters*, 114(1):018301, 2015.

[74] Mingfeng Pu, Huijun Jiang, and Zhonghuai Hou. Reentrant phase separation behavior of active particles with anisotropic janus interaction. *Soft matter*, 13(22):4112–4121, 2017.

[75] Yaouen Fily and M Cristina Marchetti. Athermal phase separation of self-propelled particles with no alignment. *Physical review letters*, 108(23):235702, 2012.

[76] Dibyendu Mandal, Katherine Klymko, and Michael R DeWeese. Entropy production and fluctuation theorems for active matter. *Physical review letters*, 119(25):258001, 2017.

[77] Lorenzo Caprini, Umberto Marini Bettolo Marconi, Andrea Puglisi, and Angelo Vulpiani. The entropy production of ornstein–uhlenbeck active particles: a path integral method for correlations. *Journal of Statistical Mechanics: Theory and Experiment*, 2019(5):053203, 2019.

[78] David Martin, Jérémy O'Byrne, Michael E Cates, Étienne Fodor, Cesare Nardini, Julien Tailleur, and Frédéric van Wijland. Statistical mechanics of active ornstein-uhlenbeck particles. *Physical Review E*, 103(3):032607, 2021.

[79] Thomas Speck. Stochastic thermodynamics for active matter. *EPL (Europhysics Letters)*, 114(3):30006, 2016.

[80] Grzegorz Szamel. Stochastic thermodynamics for self-propelled particles. *Physical Review E*, 100(5):050603, 2019.

[81] Subhasish Chaki and Rajarshi Chakrabarti. Effects of active fluctuations on energetics of a colloidal particle: Superdiffusion, dissipation and entropy production. *Physica A: Statistical Mechanics and its Applications*, 530:121574, 2019.

[82] Cesare Nardini, Étienne Fodor, Elsen Tjhung, Frédéric Van Wijland, Julien Tailleur, and Michael E Cates. Entropy production in field theories without time-reversal symmetry: quantifying the non-equilibrium character of active matter. *Physical Review X*, 7(2):021007, 2017.

[83] Suraj Shankar and M Cristina Marchetti. Hidden entropy production and work fluctuations in an ideal active gas. *Physical Review E*, 98(2):020604, 2018.

[84] Zhiyu Cao, Jie Su, Huijun Jiang, and Zhonghuai Hou. Effective entropy production and thermodynamic uncertainty relation of active brownian particles. *arXiv preprint arXiv:1907.11459*, 2019.

[85] Dominic J Skinner and Jörn Dunkel. Improved bounds on entropy production in living systems. *Proceedings of the National Academy of Sciences*, 118(18), 2021.

[86] Deepak Gupta and David A Sivak. Heat fluctuations in a harmonic chain of active particles. *Physical Review E*, 104(2):024605, 2021.

[87] Gianmaria Falasco, Richard Pfaller, Andreas P Bregulla, Frank Cichos, and Klaus Kroy. Exact symmetries in the velocity fluctuations of a hot brownian swimmer. *Physical Review E*, 94(3):030602, 2016.

[88] Howard C Berg. *E. coli in Motion*. Springer, 2004.

[89] Jens Elgeti and Gerhard Gompper. Run-and-tumble dynamics of self-propelled particles in confinement. *EPL (Europhysics Letters)*, 109(5):58003, 2015.

[90] Thibaut Demaerel and Christian Maes. Active processes in one dimension. *Physical Review E*, 97(3):032604, 2018.

[91] Kanaya Malakar, V Jemseena, Anupam Kundu, K Vijay Kumar, Sanjib Sabhapandit, Satya N Majumdar, S Redner, and Abhishek Dhar. Steady state, relaxation and first-passage properties of a run-and-tumble particle in one-dimension. *Journal of Statistical Mechanics: Theory and Experiment*, 2018(4):043215, 2018.

[92] Philip Rosenau. Random walker and the telegrapher's equation: A paradigm of a generalized hydrodynamics. *Physical Review E*, 48(2):R655, 1993.

[93] George H Weiss. Some applications of persistent random walks and the telegrapher's equation. *Physica A: Statistical Mechanics and its Applications*, 311(3-4):381–410, 2002.

[94] Martin R Evans and Satya N Majumdar. Run and tumble particle under resetting: a renewal approach. *Journal of Physics A: Mathematical and Theoretical*, 51(47):475003, 2018.

[95] Abhishek Dhar, Anupam Kundu, Satya N Majumdar, Sanjib Sabhapandit, and Grégory Schehr. Run-and-tumble particle in one-dimensional confining potentials: steady-state, relaxation, and first-passage properties. *Physical Review E*, 99(3):032132, 2019.

[96] Luca Angelani. Run-and-tumble particles, telegrapher's equation and absorption problems with partially reflecting boundaries. *Journal of Physics A: Mathematical and Theoretical*, 48(49):495003, 2015.

[97] Nitzan Razin. Entropy production of an active particle in a box. *Physical Review E*, 102(3):030103, 2020.

[98] Nicolaas Godfried Van Kampen. *Stochastic processes in physics and chemistry*, volume 1. Elsevier, 1992.

[99] Massimiliano Esposito, Katja Lindenberg, and Chris-

tian Van den Broeck. Entropy production as correlation between system and reservoir. *New Journal of Physics*, 12(1):013013, 2010.

[100] Heinz Georg Schuster. *Nonequilibrium statistical physics of small systems: Fluctuation relations and beyond.* John Wiley & Sons, 2013.

[101] Sheldon Katz, Joel L Lebowitz, and H Spohn. Phase transitions in stationary nonequilibrium states of model lattice systems. *Physical Review B*, 28(3):1655, 1983.

[102] Christian Maes. Local detailed balance. *SciPost Physics Lecture Notes*, page 032, 2021.

[103] Yuting I Li and Michael E Cates. Steady state entropy production rate for scalar langevin field theories. *Journal of Statistical Mechanics: Theory and Experiment*, 2021(1):013211, 2021.

[104] Daniel M Busiello, Deepak Gupta, and Amos Maritan. Entropy production in systems with unidirectional transitions. *Physical Review Research*, 2(2):023011, 2020.

[105] Crispin W Gardiner et al. *Handbook of stochastic methods*, volume 3. springer Berlin, 1985.

[106] Daniel M Busiello and Carlos Fiore. Hyperaccurate bounds in discrete-state markovian systems. *arXiv preprint arXiv:2205.00294*, 2022.

[107] Pawel Romanczuk, Markus Bär, Werner Ebeling, Benjamin Lindner, and Lutz Schimansky-Geier. Active brownian particles. *The European Physical Journal Special Topics*, 202(1):1–162, 2012.

[108] Derek Frydel. Intuitive view of entropy production of ideal run-and-tumble particles. *Physical Review E*, 105(3):034113, 2022.

[109] Derek Frydel. Entropy production of active particles in underdamped regime. *arXiv preprint arXiv:2211.02082*, 2022.